ISCI, Volume *15*

Supplemental Information

Cortical Correlates of Locomotor Muscle Synergy Activation in Humans: An Electroencephalographic Decoding Study

Hikaru Yokoyama, Naotsugu Kaneko, Tetsuya Ogawa, Noritaka Kawashima, Katsumi Watanabe, and Kimitaka Nakazawa

Supplemental Information

Supplemental Figures

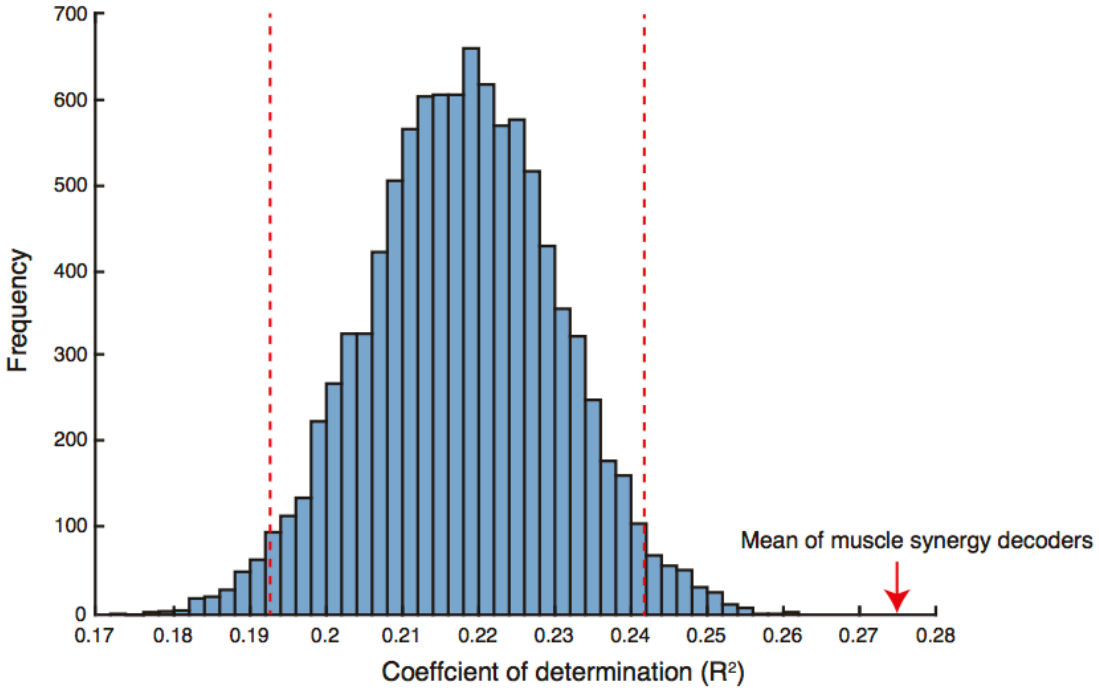

Figure S1. Histogram of the distribution of the across-participant mean of the overall decoding accuracy of individual muscle decoders from the same number of randomly selected muscles as the muscle synergies. Related to Figure 5. Vertical red lines indicate the 95% confidence intervals. The red arrow indicates the across-participant mean of the overall decoding accuracy of muscle synergy decoders.

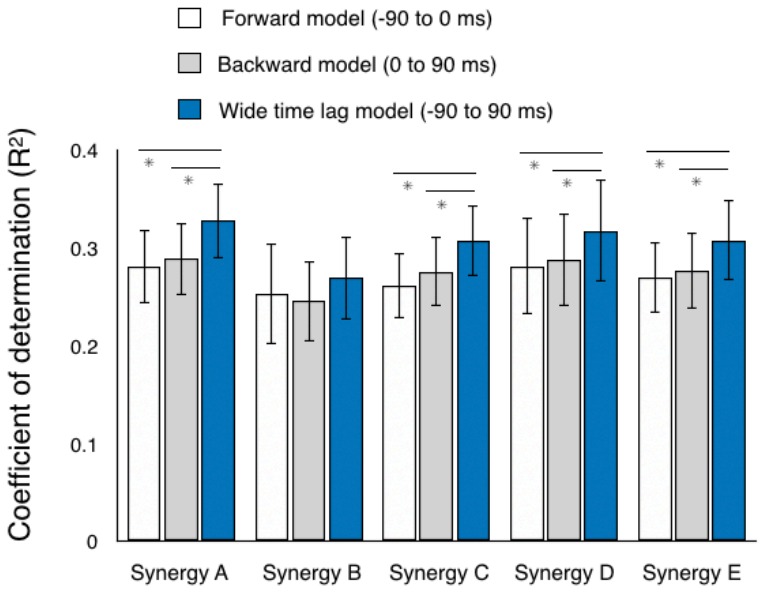

Figure S2. Decoding accuracy (coefficient of determination) of muscle synergy decoders in three different decoder types (Forward, Backward and Wide time lag models). Related to Figure 5. The mean and SEM across all participants are shown. Asterisks indicate significant differences (*: $p < 0.05$, FDR corrected for multiple comparisons; see Table S7 for detailed statistical values).

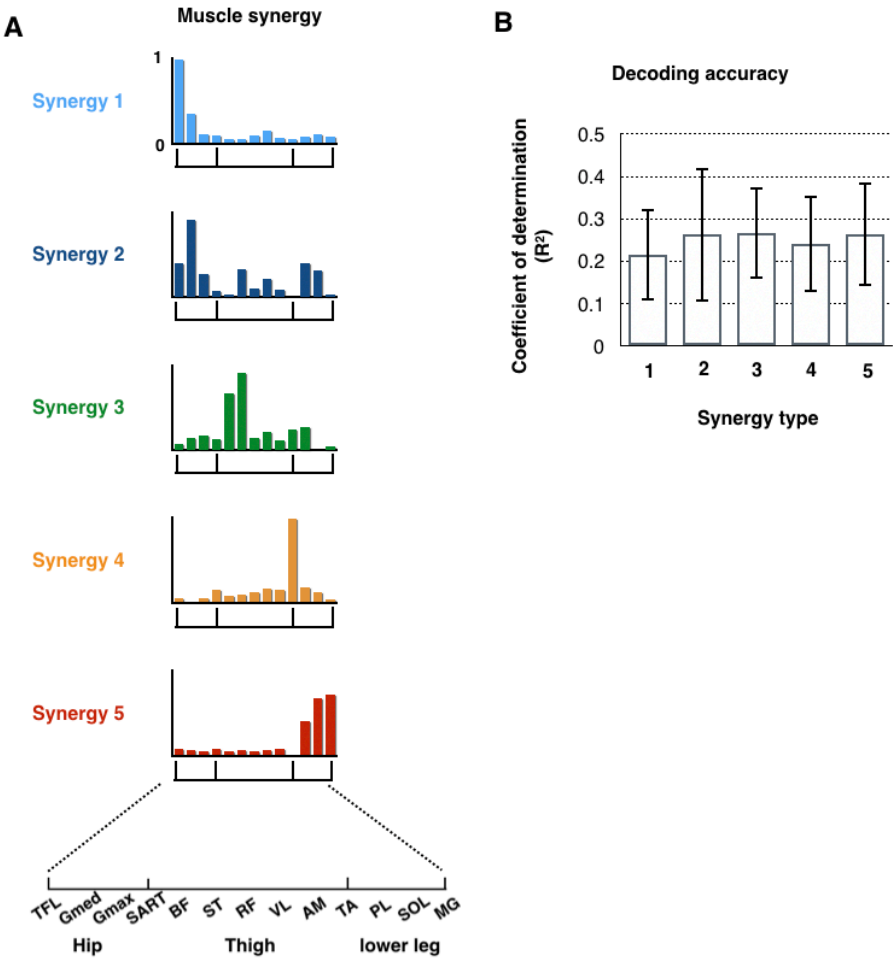

Figure S3. Five extracted types of locomotor muscle synergies from non-normalized muscle activity (A) and decoding accuracy for the muscle synergies (B). Related to Figure 5. (A) Averaged muscle synergies (bars, spatial muscle weightings) across participants in each type are shown. Each bar height represents the relative level of activation of each muscle synergy. An enlarged view of the x-axis is shown at the bottom. (B) The mean and SD of the decoding accuracy (coefficient of determination) across participants for each muscle synergy type are shown.

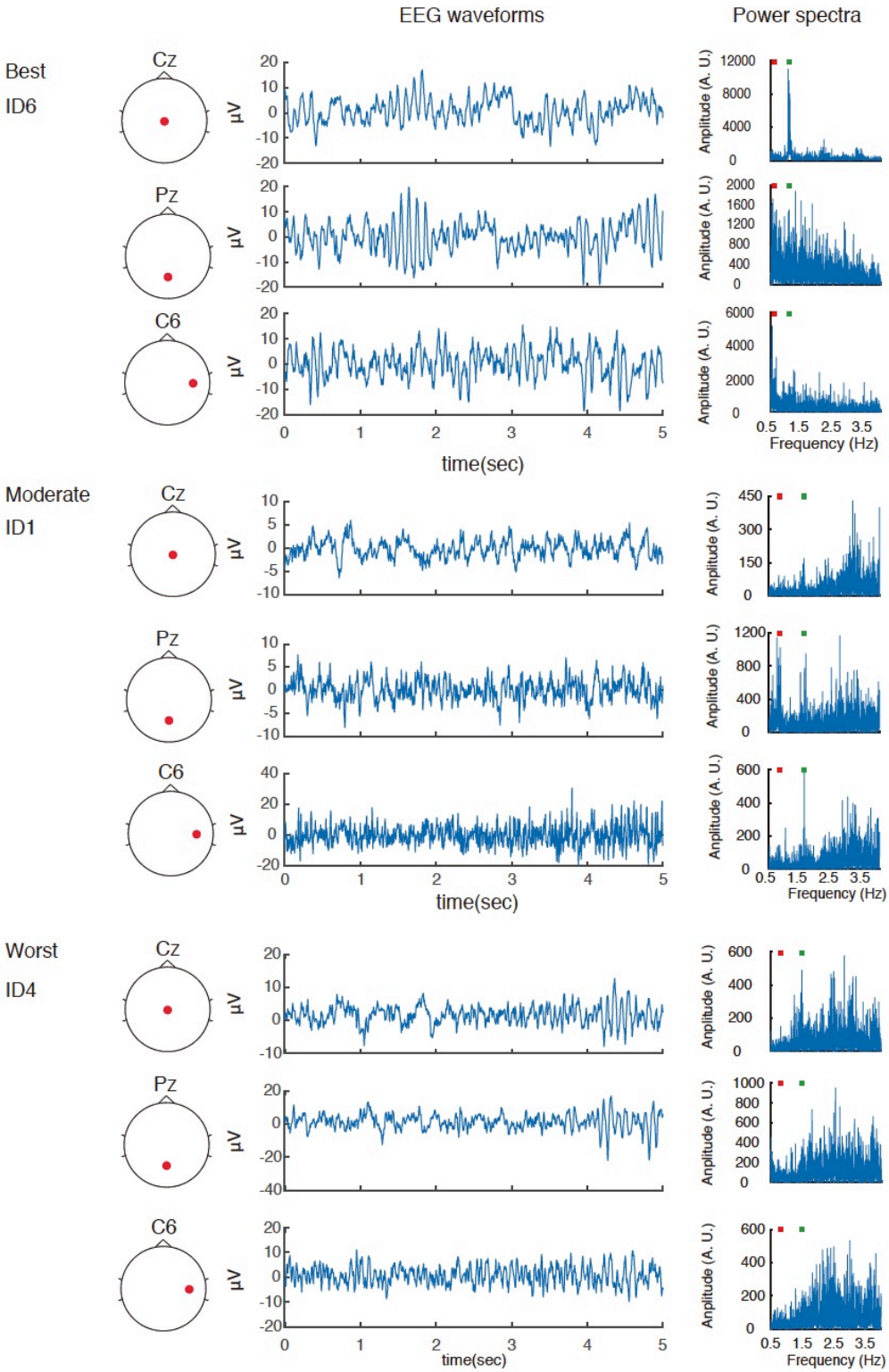

Figure S4. Examples of EEG data from three electrodes (Cz, Pz, C6), for the diversity of their spatial localizations (top, back, and right side of the head, respectively), from participants who showed the best, moderate, and worst decoding accuracies, respectively. Related to Figure 5 and Figure7. The central column shows 5 seconds of EEG signals after artifact subspace reconstruction (ASR) just before low-pass filtering (4 Hz) to obtain slow cortical potentials. The

right column shows the power spectra of the electrodes in the delta band (0.5–4 Hz). Red and green squares indicate their stride and step frequency, respectively.

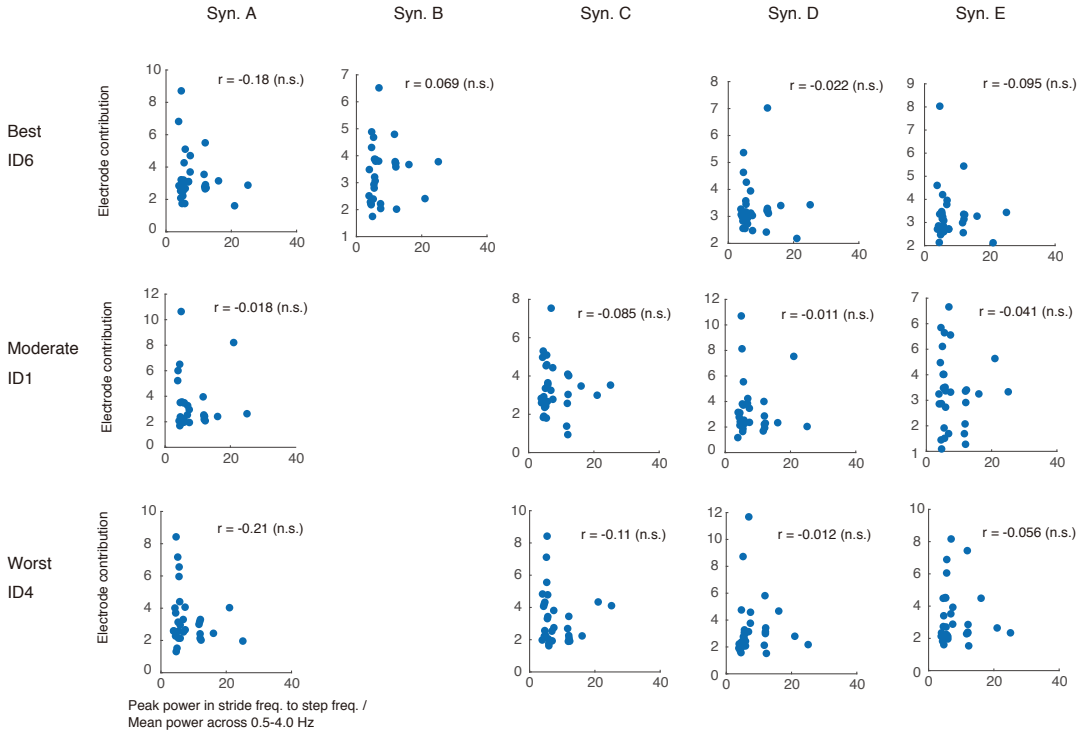

Figure S5. Relation between electrode contribution to the decoding and movement artifact size of participants who showed the best, moderate and worst decoding accuracy. Related to Figure 5 and Figure7. Each plot indicate each electrode data. Correlation coefficients are shown.

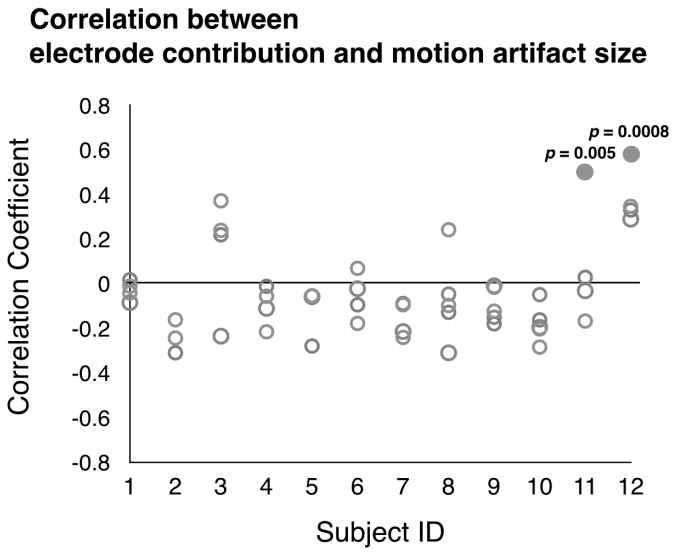

Figure S6. Correlation between electrode contribution to the decoding and movement artifact size for all muscle synergy decoders in all participants. Related to Figure 5 and Figure7. Each plot indicates the correlation value for each muscle synergy decoder. Open and filled circles indicate statistically non-significant and significant correlation values, respectively.

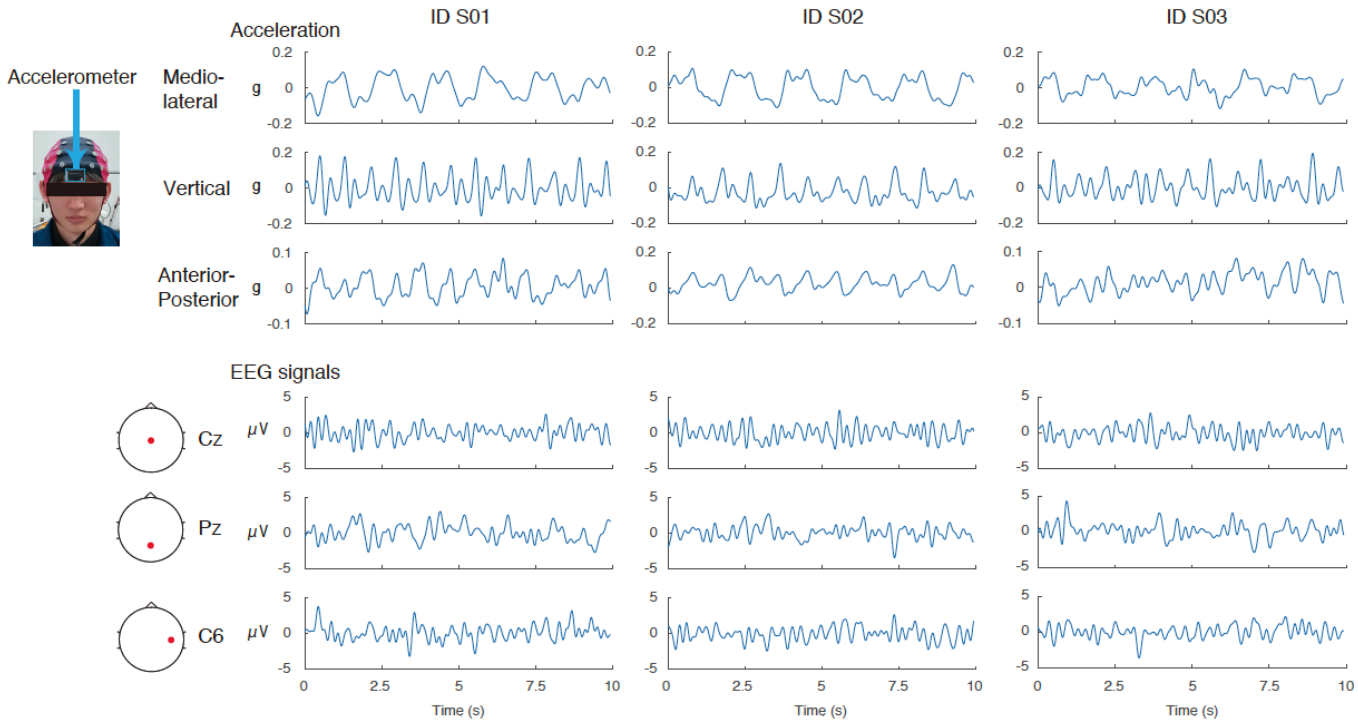

Figure S7. Time courses of head accelerations (mediolateral, vertical, and anterior-posterior), and EEG signals (slow cortical potentials) from three electrodes (Cz, Pz, C6), for the diversity of their spatial localizations (top, back, and right side of the head, respectively), from all three participants in the supplemental experiment. Related to Figure 5 and Figure7.

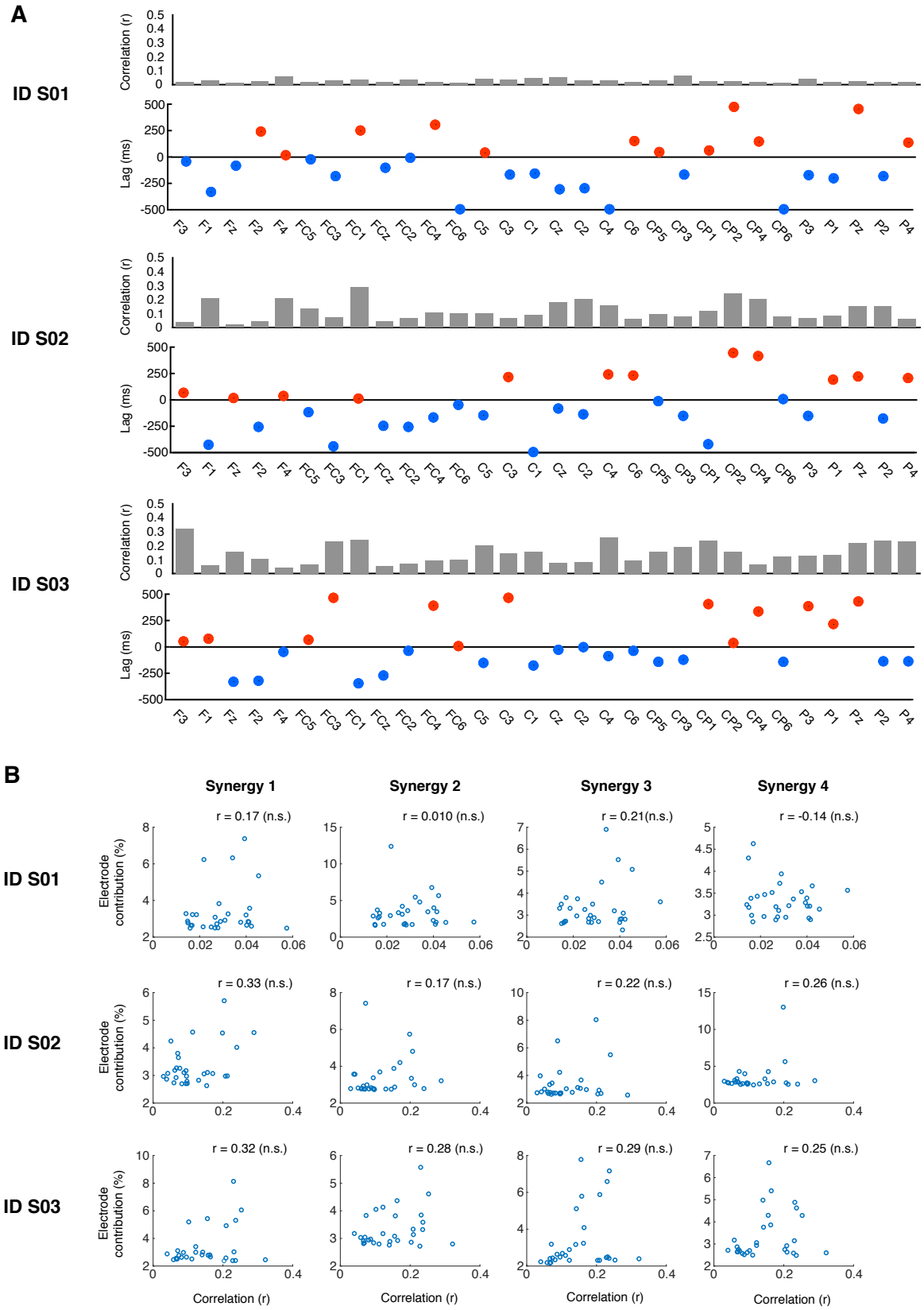

Figure S8. Cross-correlation results between vertical head accelerations and slow cortical potentials. Related to Figure 5 and Figure7. (A) Peak correlation coefficient values are shown in the bar graphs. Time lags at the peak correlation values are shown in the plot graphs. Red plots indicate that EEG signals are preceding the head accelerations; blue plots indicate that head accelerations are preceding the EEG signals. (B) Relation between the peak correlation values of the cross-correlation analysis and electrode contribution in all electrodes in each muscle synergy decoder.

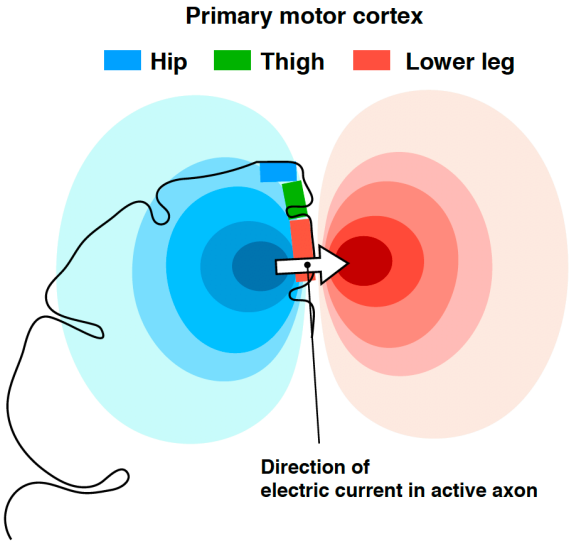

Figure S9. Schematic illustration of the electrical source in the left primary motor cortex corresponding to the right lower leg muscle area and the resulting electrical field in the brain. Related to Figure7. Blue, green, and red rectangles represent the cortical areas corresponding to the hip, thigh, and lower leg muscles, respectively. The white arrow indicates direction of electric current of an electric source (i.e., neural column). Darker areas of color indicate a stronger electric field. Red and blue areas indicate positive and negative values, respectively.

Supplemental tables

Table S1. Characteristics of each type of locomotor muscle synergy. Related to Figure 3.

Type	Activation timing	Major muscles
Synergy A	Mid stance phase	TFL, Gmed, and GM
Synergy B	Mid swing phase and early stance phase	ST, RF, VL, AM, and TA
Synergy C	Last swing to initial stance phase	BF, ST
Synergy D	Mid swing phase and transition from the stance phase to the swing phase	AM, TA
Synergy E	Latter half of stance phase	SOL and MG

Table S2. Summary of statistical analyses for comparisons of decoding accuracy among each ROI and all electrodes for Synergy A. Related to Figure 7.

Method	Pair	Value
ANOVA		$F_{4,48} = 19.15$, $p = 1.8\times10^{-9}$
Multiple t-test with FDR correction	Frontal vs. Cental	p = 0.50
Multiple t-test with FDR correction	Frontal vs. Lateral	p = 0.33
Multiple t-test with FDR correction	Frontal vs. Parietal	p = 0.29
Multiple t-test with FDR correction	Frontal vs. All	p = 0.00010
Multiple t-test with FDR correction	Central vs. Lateral	p = 0.16
Multiple t-test with FDR correction	Central vs. Parietal	p = 0.13
Multiple t-test with FDR correction	Central vs. All	p = 6.3e-05
Multiple t-test with FDR correction	Lateral vs. Parietal	p = 0.52
Multiple t-test with FDR correction	Lateral vs. All	p = 7.1e-05
Multiple t-test with FDR correction	Parietal vs. All	p = 0.00010

Table S3. Summary of statistical analyses for comparisons of decoding accuracy among each ROI and all electrodes for Synergy B. Related to Figure 7.

Method	Pair	Value
ANOVA		$F_{4,20} = 11.32$, $p = 5.8\times10^{-5}$
Multiple t-test with FDR correction	Frontal vs. Cental	p = 0.16
Multiple t-test with FDR correction	Frontal vs. Lateral	p = 0.74
Multiple t-test with FDR correction	Frontal vs. Parietal	p = 0.74
Multiple t-test with FDR correction	Frontal vs. All	p = 0.027
Multiple t-test with FDR correction	Central vs. Lateral	p = 0.16
Multiple t-test with FDR correction	Central vs. Parietal	p = 0.46
Multiple t-test with FDR correction	Central vs. All	p = 0.027
Multiple t-test with FDR correction	Lateral vs. Parietal	p =0.47
Multiple t-test with FDR correction	Lateral vs. All	p = 0.027
Multiple t-test with FDR correction	Parietal vs. All	p = 0.036

Table S4. Summary of statistical analyses for comparisons of decoding accuracy among each ROI and all electrodes for Synergy C. Related to Figure 7.

Method	Pair	Value
ANOVA		$F_{4,36} = 17.57$, $p = 4.4\times10^{-8}$
Multiple t-test with FDR correction	Frontal vs. Cental	p = 0.80
Multiple t-test with FDR correction	Frontal vs. Lateral	p = 0.45
Multiple t-test with FDR correction	Frontal vs. Parietal	p = 0.77
Multiple t-test with FDR correction	Frontal vs. All	p = 0.0013
Multiple t-test with FDR correction	Central vs. Lateral	p = 0.77
Multiple t-test with FDR correction	Central vs. Parietal	p = 0.77
Multiple t-test with FDR correction	Central vs. All	p = 0.00026
Multiple t-test with FDR correction	Lateral vs. Parietal	p = 0.99
Multiple t-test with FDR correction	Lateral vs. All	p = 0.00023
Multiple t-test with FDR correction	Parietal vs. All	p = 0.00023

Table S5. Summary of statistical analyses for comparisons of decoding accuracy among each ROI and all electrodes for Synergy D. Related to Figure 7.

Method	Pair	Value
ANOVA		$F_{4,24} = 9.18$, $p = 0.00012$
Multiple t-test with FDR correction	Frontal vs. Cental	p = 0.28
Multiple t-test with FDR correction	Frontal vs. Lateral	p = 0.93
Multiple t-test with FDR correction	Frontal vs. Parietal	p = 0.82
Multiple t-test with FDR correction	Frontal vs. All	p = 0.0069
Multiple t-test with FDR correction	Central vs. Lateral	p = 0.30
Multiple t-test with FDR correction	Central vs. Parietal	p = 0.68
Multiple t-test with FDR correction	Central vs. All	p = 0.0074
Multiple t-test with FDR correction	Lateral vs. Parietal	p = 0.82
Multiple t-test with FDR correction	Lateral vs. All	p = 0.0069
Multiple t-test with FDR correction	Parietal vs. All	p = 0.0069

Table S6. Summary of statistical analyses for comparisons of decoding accuracy among each ROI and all electrodes for Synergy E. Related to Figure 7.

Method	Pair	Value
ANOVA		$F_{4,52} = 16.11$, $p = 1.22\times10^{-8}$
Multiple t-test with FDR correction	Frontal vs. Cental	p = 0.023
Multiple t-test with FDR correction	Frontal vs. Lateral	p = 0.57
Multiple t-test with FDR correction	Frontal vs. Parietal	p = 0.30
Multiple t-test with FDR correction	Frontal vs. All	p = 0.00033
Multiple t-test with FDR correction	Central vs. Lateral	p = 0.053
Multiple t-test with FDR correction	Central vs. Parietal	p = 0.0082
Multiple t-test with FDR correction	Central vs. All	p = 0.0013
Multiple t-test with FDR correction	Lateral vs. Parietal	p = 0.84
Multiple t-test with FDR correction	Lateral vs. All	p = 0.0012
Multiple t-test with FDR correction	Parietal vs. All	p = 0.00040

Table S7. Summary of statistical analyses for comparisons of decoding accuracy between three types of decoders (Forward, Backward and Wide time lag decoders). Related to Figure 5. See also Figure S2.

Method	Statistical value				
	Synergy A	Synergy B	Synergy C	Synergy D	Synergy E
ANOVA	$F_{2,24} = 19.08$, $p = 1.1\times10^{-5}$	$F_{2,10} = 2.15$, $p = 0.168$	$F_{2,18} = 32.99$, $p = 9.6\times10^{-7}$	$F_{2,12} = 16.87$, $p = 0.00033$	$F_{2,26} = 14.35$, $p = 6.3\times10^{-5}$
Multiple t-test with FDR correction (Forward vs. Backward)	p = 0.6803	-	p = 0.054	p = 0.65	p = 0.71
Multiple t-test with FDR correction (Forward vs. Wide time lag)	p = 9.1e-06	-	p = 0.00015	p = 0.0060	p = 0.0030
Multiple t-test with FDR correction (Backward vs. Wide time lag)	p = 0.0056	-	p = 0.0013	p = 0.012	p = 0.00045

Table S8. Summary of decoding accuracy in the supplemental experiment. Related to Figure 5 and Figure 7. See also Figure S7 and Figure S8.

	ID-S01	ID-S02	ID-S03	All muscle synergies from three participants
R^2 (Mean (SD))	0.29 (0.038)	0.21 (0.035)	0.20 (0.062)	0.23 (0.060)

Transparent Methods

Experimental model and subject details

Participants

In this study, we conducted two experiments: 1) the main experiment and 2) the supplemental experiment. Twelve healthy male volunteers (age, 23–31 years) participated in the main experiment. Additionally, three healthy male volunteers (age, 24–28 years) participated in the supplemental experiment. Each participant provided written informed consent. The experiments were performed in accordance with the Declaration of Helsinki and with the approval of the Ethics Committee of the Graduate School of Arts and Sciences, University of Tokyo.

Method details

Main experiment

Experimental design and setup

Participants walked on a treadmill (Bertec, Columbus, OH, USA) at 0.55 m/s for 7 min 30 seconds. The last seven minutes of data were used for the analysis. The slow walking speed was chosen based on two previous studies examining the effects of walking speed on movement artifacts in EEG signals (Kline et al., 2015; Nathan and Contreras-Vidal, 2016): Kline et al. (2015) used an experimental method to isolate and record independent movement artifacts with a silicone swim cap (nonconductive material), and reported large movement artifacts at walking speeds faster than 0.8 m/s. A study that analyzed relationships between head acceleration and motion artifacts in EEG signals indicated that recordings were robust at gait speeds below 3.0 km/h (0.83 m/s) (Nathan and Contreras-Vidal, 2016). As a static baseline condition, the participants sat on a chair for two minutes.

Data collection

Three-dimensional ground reaction forces (GRF) were recorded from force plates under the right and left belts of the treadmill (sampling rate: 1000 Hz). GRF data were smoothed with a low-pass filter (zero-lag Butterworth filter, 5 Hz cutoff). MATLAB 2016b (MathWorks, Natick, MA, USA) was used to perform all the post-processing analyses offline.

Surface electromyographic (EMG) signals were recorded from the following 13 leg muscles on the right side using a wireless EMG system (Trigno Wireless System, DelSys Inc., Boston, MA, USA): tensor fasciae latae (TFL), gluteus maximus (GM), gluteus medius (Gmed), sartorius (SART), biceps femoris (BF), semitendinosus (ST), rectus femoris (RF), vastus lateralis (VL), adductor magnus (AM), tibialis anterior (TA), peroneus longus (PL), soleus (SOL), and gastrocnemius medialis (MG). EMGs were amplified (with 300 gain preamplifier), band-pass filtered (20–450 Hz), and sampled at 1000 Hz.

A 64-channel EEG cap (Waveguard original, ANT Neuro b.v., Enschede, Netherlands) and a mobile EEG amplifier (eego sports, ANT Neuro b.v., Enschede, Netherlands) were used to record EEG signals at a sampling frequency of 500 Hz. Arrangement of the electrodes was according to the international 10–20 electrode system. EEG signals were referenced to CPz and a ground electrode was placed on AFz. Electrode impedances were kept below 30 kΩ (10 kΩ in most electrodes), which was substantially below the recommended impedance (below 50 kΩ) for the high-impedance EEG amplifier. Peripheral channels, which are prone to contamination by facial/cranial muscle activity and eye blinks, were removed from the offline analysis (channels labeled Fp, AF, FT, T, TP, O, PO, and F5-8, P5-8) (Bulea et al., 2014), resulting in the 30 channels presented in Figure 1.

EMG processing and extraction of locomotor muscle synergies

Figure 2 shows an overview of our decoding methodology. From the recorded EMG signals, EMG envelopes and muscle synergies were used for the neural decoding analysis.

First, the recorded EMG data were high-pass filtered (zero-lag fourth-order Butterworth at 30 Hz), demeaned, full-wave rectified, and smoothed with a low-pass filter (zero-lag fourth-order Butterworth at 4 Hz cutoff) to obtain EMG envelopes (Clark et al., 2010). EMG envelopes were resampled at 100 Hz. The amplitude of EMG envelopes for each muscle was normalized to the maximum value for that muscle during the walking task. Muscle synergies were extracted from the processed EMG envelopes using non-negative matrix factorization (NMF) (Clark et al., 2010; d'Avella and Bizzi, 2005; Dominici et al., 2011; Lee and Seung, 1999; Yokoyama et al., 2016). For each participant, muscle synergies were extracted from the EMG dataset organized as a matrix with 13 muscles × 42000 variables (i.e., 100 Hz × 420 sec [7 min]). Using NMF, the EMG matrix (*M*) was decomposed into spatial muscle weightings (*S*), which correspond to the muscle synergies and their temporal activations (*C*) according to formula (1):

$$M = S \cdot C + E \quad (1)$$

where *M* (*m* × *t* matrix, where *m* is the number of muscles and *t* is the number of samples in the EMG data matrix) is a linear combination of muscle synergies, *S* (*m* × $N_{synergy}$ matrix, where $N_{synergy}$ is the number of muscle synergies), and their temporal activation patterns, *C* ($N_{synergy}$ × *t* matrix), and *E* is the residual error matrix. The number of muscle synergies, $N_{synergy}$, was determined by iterating each possible $N_{synergy}$ from 1 to 10. For each $N_{synergy}$, the goodness of fit was evaluated based on the variance accounted for (VAF) (Torres-Oviedo et al., 2006). Based on the VAF, the optimal $N_{synergy}$ was defined as the minimum value fulfilling two criteria: (1) the number of muscle synergies achieving VAF > 90% (Torres-Oviedo et al., 2006), and (2) the number to which adding an additional muscle synergy did not increase VAF by > 5% (Frere and Hug, 2012). Then,

we clustered the extracted muscle synergies using hierarchical clustering analysis to examine the extracted types of muscle synergies (Ward's method, correlation distance) based on muscle weightings, as in our previous studies (Yokoyama et al., 2017a; Yokoyama et al., 2016; Yokoyama et al., 2017b). The gap statistic method was used to define the optimal number of clusters (Tibshirani et al., 2001).

EEG pre-processing

In the current study, fluctuations in the amplitude of slow cortical potentials (0.5 – 4 Hz in the time domain) were used for the neural decoding analysis (Figure 2) based on a similar methodology used in previous studies (Bradberry et al., 2010; Contreras-Vidal et al., 2018; Nakanishi et al., 2017; Presacco et al., 2012; Presacco et al., 2011). EEG data analysis was performed using custom programs in MATLAB incorporating functions of EEGLAB 14.1b (Delorme and Makeig, 2004). The EEG signals were band-pass filtered between 0.5−100 Hz with a Butterworth filter (fourth-order). The "cleanline" function in EEGLAB was used to remove power line noise (50 Hz). Next, the EEG signals were resampled at 100 Hz. Then, we checked noisy EEG channels based on two criteria adopted from a previous study (Gwin et al., 2011): 1) standard deviation greater than 1000 μV, and 2) kurtosis of more than five standard deviations from the mean. In this study, no EEG electrode satisfied the criteria in all the participants. Since various types of artifacts were potentially introduced in the EEG data, we used an artifact rejection method called Artifact Subspace Reconstruction (ASR) (Mullen et al., 2015) in EEGLAB to remove artifacts derived from walking, eye blinks, muscle, and heart activity. Next, the cleaned EEG signals were low-pass filtered at 4 Hz with a zero-phase Butterworth filter (fourth-order) and re-referenced to a common average reference. Finally, the amplitude of each electrode was normalized by calculating the standard z-score.

Neural decoding of muscle synergy and individual muscle activation

To continuously decode the activation of muscle synergies and individual muscles from the slow cortical potentials, we designed a time-embedded (10 lags, corresponding to 0 ms to -90 ms) linear decoding model, called the Wiener filter (Bradberry et al., 2010; Carmena et al., 2003; Presacco et al., 2011), for the muscle synergy and EMG envelope data. The linear model is given by:

$$y(t) = b + \sum_{i=1}^{N_{electrode}} \sum_{j=1}^{L} W_{ij} \cdot x_i[t-(j-1)] + e(t) \quad (2)$$

where $y(t)$ is the predicted time series activation of each muscle synergy or EMG envelope at time t, b is the intercept, $N_{electrode}$ (= 30) is the number of electrodes, L (=10) is the number of time lags, $x(t)$ is the normalized slow cortical potentials at electrode i at time t, W_{ij} is the weights at electrode i and time lag j, and $e(t)$ is the residual error. The time lag was selected to use the cortical information ahead of the muscle activity because we were interested in examining the cortical descending control of muscle activity. The maximum time lag (-90 ms) was chosen based on the traveling time of the cortical command to the muscles examined by TMS (~35−40 ms) (Nielsen et al., 1995; Terao et al., 2000). Thus, we set the time lag to sufficiently contain the traveling time. The parameters of the model were calculated with multidimensional generalized linear regression (Bradberry et al., 2010; Carmena et al., 2003; Presacco et al., 2011) using the "glm" function in MATLAB (Gaussian distribution condition). Neural decoders were designed separately for each participant and each decoded parameter (i.e., each muscle synergy and each EMG envelope).

In addition to the above-explained forward decoder (-90 to 0 ms, forward model), we performed decoding analyses of muscle synergy activation using two additional types of decoders, which used positively time-lagged information (0 to 90 ms, backward model) and widely time-lagged information (-90 to 90 ms, wide time lag model).

For assessing the predictive accuracy of each decoder, a seven-fold cross-validation procedure was performed. Thus, the data recorded during the 7 min walking task were divided into 7 segments (1 min each). Six segments were used for training data while the remaining segment was used for testing the decoding model. In the cross-validation, the temporal activation patterns of muscle synergies (C in equation (1)) for the test data were calculated using the NMF algorithm initialized with the spatial weightings of muscle synergies (S in equation (1)) extracted from the training data and updating only the temporal activation patterns of the synergies to reconstruct the muscle activation patterns of test data (Berger et al., 2013; Clark et al., 2010; d'Avella et al., 2006; Yokoyama et al., 2016). The EEG signals for the test data were normalized by subtracting a mean value from the training data and then dividing by the standard deviation of the training data. This procedure was repeated for all possible combinations (i.e., seven times). Coefficient of determination (R^2) were calculated between the real activation and the decoded activation at each decoder in each iteration. To compare the overall decoding accuracy between the two types of decoders (muscle synergy decoders vs. individual muscle decoders), overall R^2 values were calculated for each type per participant. To minimize the effects of skewness in the sampling distributions on the correlation coefficients, each coefficient of determination value was averaged after Fisher's Z-transformation (Corey et al., 1998). After averaging, the Z-values were back-transformed to the scale of Pearson's r values.

The difference in the number of decoders (individual muscles: 13, muscle synergies: 3−5 depending on participants) may have possibly affected the comparisons of the overall decoding accuracy, as the sample mean of the larger sample size more accurately estimates the population mean. To overcome this issue, the overall decoding accuracy was calculated using the same number of randomly sampled individual muscle decoders with muscle synergies from 13 muscles per participants (sampling without replacement). In this analysis, the Z-transformed decoding accuracy values were randomly sampled and averaged. We then calculated the across-participant mean of the overall decoding accuracy for individual muscle decoders. The procedure was iterated 10000 times, and we calculated the 95% confidence interval of the distribution of the 10000 values of the across-participant mean of the overall decoding accuracy of individual muscles. Then, we tested whether the across-participant mean of the overall decoding accuracy for muscle synergy decoders was larger than the 95% confidence interval.

Chance levels of neural decoding were evaluated by randomizing the EEG phase (Theiler et al., 1992). Phase-randomized EEG signals were generated using the fast Fourier transform of a time series throughout the recording duration to randomize the phase in the Fourier domain while keeping the power spectrum unchanged; then the inverse Fourier transform was performed to back to the time domain. After phase-randomization, the power spectrum was preserved in the surrogate data, but the phase relation to the muscle activity was disrupted. When decoding from the time-domain EEG signals, it is assumed that the signals are phase-locked to muscle activity and that a randomization of the phase can provide a chance level of the decoding accuracy. The same decoding procedure was performed using the phase-randomized EEG signals. We generated 100 phase-randomized EEG datasets for each participant

and performed neural decoding using each randomized dataset to obtain confidence intervals for the decoding accuracy.

Analysis of relationships between muscle synergy decoders and individual muscle decoders

We reconstructed individual muscle activations by summing the outputs of each decoded muscle synergy to test whether the variability in decoding accuracy in individual muscles would be reproduced by individual muscle activations indirectly decoded from muscle synergy activations decoded from muscle synergy decoders. The output of a decoded muscle synergy was explained by the product of the muscle weighting component and the decoded temporal activation pattern from the slow cortical potentials. Next, the decoding accuracy of the indirectly decoded individual muscle activation through the decoded muscle synergies were assessed.

To examine the weight of each muscle decoder (W_{muscle}) based on those of the muscle synergy decoders (W_{syn}), a 300-dimensional weight of an individual muscle decoder was reconstructed as a linear combination of the weights of the muscle synergy decoders with non-negative coefficients (W_{muscle}', conceptual schema presented in Figure 6C). The non-negative least squares problem was solved by the "lsqnonneg" function in MATLAB. The similarity of the weights of the original and reconstructed individual muscle decoders (i.e., W_{muscle} and W_{muscle}', respectively) was evaluated using Pearson's *r,* calculated from the decoder data of all participants.

Contribution of each electrode to decoding

To evaluate the spatial contributions of cortical activity to predict muscle synergy activations, we calculated the contribution of each electrode from the weights of the decoding model as determined in a previous study (Chao et al., 2010):

$$\%T_k = \frac{\sum_{j=1}^{L}|w_{kj}|}{\sum_{i=1}^{N_{electrode}}\sum_{j=1}^{L}|w_{ij}|} \times 100; \quad (3)$$

for all *k* from 1 to $N_{electrode}$, where $\%T_k$ is the percentage contribution of each EEG electrode *k*.

In addition, we divided the electrodes into four major ROIs to examine the individual contribution of each area to the decoding. The ROIs were the frontal area (F3, F1, Fz, F2, F4, FC3, FC1, FCz, FC2, and FC4), central area (FC1, FCz, FC2, C3, C1, Cz, C2, C4, CP1, and CP2), lateral area (FC5, FC3, FC4, FC6, C5, C6, CP5, CP3, CP4, and CP6), and parietal area (CP3, CP1, CP2, CP4, P3, P1, Pz, P2, and P4). Using the same procedure as for the full electrodes, the decoding accuracy of each muscle synergy activation was separately calculated using the electrode set in each ROI.

Effects of amplitude normalization of EMG signals

To examine the effect of amplitude normalization of EMG signals on the decoding of muscle synergy activation, we also extracted muscle synergies from non-normalized EMG activity and performed decoding analyses using the muscle synergy activation. We performed the same procedures for muscle synergy extraction and activation decoding as those used those for muscle synergies extracted from normalized EMGs.

Effects of motion artifact in EEG

The spectra of the EEG signals were analyzed using the fast Fourier transform (FFT) via the fft function in Matlab. Default setting parameters of the fft function were used (FFT size was set to

the length of the EEG signal rounded up to the next power of two). The power spectra of EEGs, which are affected by motion artifact during walking, exhibit the power peaks around the stride and step frequencies due to head motion (Arad et al., 2018; Kline et al., 2015; Nathan and Contreras-Vidal, 2016). Therefore, we calculated the relative power between the peak power in frequency from the stride to step frequencies and the mean power in the delta band frequency (0.5−4.0 Hz) as a rough indicator of artifact size of each electrode. Then, relationships between the artifact size and electrode contribution to the decoding, defined by formula (3), were examined using Pearson's correlation coefficient in each muscle synergy decoder per participant.

Supplemental experiment

Three participants walked on a treadmill under the same experimental conditions used in the main experiment. In this supplemental experiment, we measured tri-axial head accelerations with a 1000 Hz sampling frequency in addition to obtaining EEG, EMG, and GRF data under the same data recording conditions. An accelerometer (Trigno Wireless System, DelSys Inc., Boston, MA, USA) was attached to the participant's forehead along the midline of the nose (Figure S7), as described in previous studies (Kline et al., 2015; Nathan and Contreras-Vidal, 2016), to measure the best estimate of the head acceleration without any interfering EEG recordings.

Using the same analyses performed for the main experiment data, we extracted muscle synergies from EMG signals and then performed the decoding analysis of muscle synergy activation from slow cortical potentials obtained from the EEG signals. The acceleration signals were band-pass filtered between 0.5−4 Hz with a Butterworth filter (fourth-order) to examine the effects of head acceleration on the slow cortical potentials of EEGs. Then, the acceleration

data were resampled at 100 Hz to match the sampling frequency for the slow cortical potentials. If the head acceleration affected the activation patterns of the slow cortical potentials, the two signals showed a correlation with the time lag, in which the head movement preceded the slow cortical potentials. Because movement artifacts are mainly caused by vertical head accelerations (Kline et al., 2015), we calculated the cross-correlation between the time series of vertical head accelerations and slow cortical potentials at each electrode. The maximum correlation between the vertical head accelerations and the slow cortical potentials were examined in a time lag range from -500 to 500 ms so as not to exceed the step duration (approximately 600—900 ms depending on the participants). Finally, we used Pearson's correlation to examine the relationships between the electrode contribution to the decoding and the maximum correlation of the cross-correlation analysis in all the electrodes in each muscle synergy decoder.

Quantification and statistical analysis

The differences between the overall correlation values (i.e., decoding accuracy) between the two types of decoders (muscle synergy decoder vs. individual muscle decoder) were assessed using two-tailed paired t-tests. In addition, the differences in decoding accuracy between each ROI and the full electrode set were compared using repeated measures one-way analysis of variance (ANOVA) test with multiple t-tests with FDR correction for each muscle synergy type. Before performing the t-test and ANOVA, the normality was tested and found using the Lilliefors test. For the statistical tests, the coefficient of determination values were transformed into Z-values using Fisher’s Z-transformation and the tests (i.e., t-test, ANOVA, multiple t-tests with

FDR correction) were conducted on the Fisher's Z-values. Statistical significance was set at $p < 0.05$.

Supplemental References

Arad, E., Bartsch, R.P., Kantelhardt, J.W., and Plotnik, M. (2018). Performance-based approach for movement artifact removal from electroencephalographic data recorded during locomotion. PloS One 13, e0197153.

Berger, D.J., Gentner, R., Edmunds, T., Pai, D.K., and d'Avella, A. (2013). Differences in adaptation rates after virtual surgeries provide direct evidence for modularity. J. Neurosci. 33, 12384-12394.

Bradberry, T.J., Gentili, R.J., and Contreras-Vidal, J.L. (2010). Reconstructing three-dimensional hand movements from noninvasive electroencephalographic signals. J. Neurosci. 30, 3432-3437.

Bulea, T.C., Prasad, S., Kilicarslan, A., and Contreras-Vidal, J.L. (2014). Sitting and standing intention can be decoded from scalp EEG recorded prior to movement execution. Front. Neurosci. *8*, 376.

Carmena, J.M., Lebedev, M.A., Crist, R.E., O'Doherty, J.E., Santucci, D.M., Dimitrov, D.F., Patil, P.G., Henriquez, C.S., and Nicolelis, M.A. (2003). Learning to control a brain–machine interface for reaching and grasping by primates. Plos Biol. 1, e42.

Chao, Z.C., Nagasaka, Y., and Fujii, N. (2010). Long-term asynchronous decoding of arm motion using electrocorticographic signals in monkeys. Front. Neuroeng. 3, 3.

Clark, D.J., Ting, L.H., Zajac, F.E., Neptune, R.R., and Kautz, S.A. (2010). Merging of healthy motor modules predicts reduced locomotor performance and muscle coordination complexity post-stroke. J. Neurophysiol. 103, 844-857.

Contreras-Vidal, J.L., Bortole, M., Zhu, F., Nathan, K., Venkatakrishnan, A., Francisco, G.E., Soto, R., and Pons, J.L. (2018). Neural decoding of robot-assisted gait during rehabilitation after stroke. Am. J. Phys. Med. Rehabil. *97*, 541-550.

Corey, D.M., Dunlap, W.P., and Burke, M.J. (1998). Averaging correlations: Expected values and bias in combined Pearson rs and Fisher's z transformations. J. Gen. Psychol. 125, 245-261.

d'Avella, A., and Bizzi, E. (2005). Shared and specific muscle synergies in natural motor behaviors. Proc. Natl. Acad. Sci. U. S. A. 102, 3076-3081.

d'Avella, A., Portone, A., Fernandez, L., and Lacquaniti, F. (2006). Control of fast-reaching movements by muscle synergy combinations. J. Neurosci. 26, 7791-7810.

Delorme, A., and Makeig, S. (2004). EEGLAB: an open source toolbox for analysis of single-trial EEG dynamics including independent component analysis. J. Neurosci. Methods 134, 9-21.

Dominici, N., Ivanenko, Y.P., Cappellini, G., d'Avella, A., Mondi, V., Cicchese, M., Fabiano, A., Silei, T., Di Paolo, A., Giannini, C*., et al.* (2011). Locomotor primitives in newborn babies and their development. Science 334, 997-999.

Frere, J., and Hug, F. (2012). Between-subject variability of muscle synergies during a complex motor skill. Front. Comput. Neurosci. 6, 99.

Kline, J.E., Huang, H.J., Snyder, K.L., and Ferris, D.P. (2015). Isolating gait-related movement artifacts in electroencephalography during human walking. J. Neural Eng. 12, 046022.

Lee, D.D., and Seung, H.S. (1999). Learning the parts of objects by non-negative matrix factorization. Nature 401, 788-791.

Mullen, T.R., Kothe, C.A., Chi, Y.M., Ojeda, A., Kerth, T., Makeig, S., Jung, T.-P., and Cauwenberghs, G. (2015). Real-time neuroimaging and cognitive monitoring using wearable dry EEG. IEEE Trans. Biomed. Eng. *62*, 2553-2567.

Nakanishi, Y., Yanagisawa, T., Shin, D., Kambara, H., Yoshimura, N., Tanaka, M., Fukuma, R., Kishima, H., Hirata, M., and Koike, Y. (2017). Mapping ECoG channel contributions to trajectory and muscle activity prediction in human sensorimotor cortex. Sci. Rep. 7, 45486.

Nathan, K., and Contreras-Vidal, J.L. (2016). Negligible motion artifacts in scalp electroencephalography (EEG) during treadmill walking. Front. Hum. Neurosci. 9, 708.

Nielsen, J., Petersen, N., and Ballegaard, M. (1995). Latency of effects evoked by electrical and magnetic brain stimulation in lower limb motoneurones in man. J. Physiol. 484, 791-802.

Presacco, A., Forrester, L.W., and Contreras-Vidal, J.L. (2012). Decoding intra-limb and inter-limb kinematics during treadmill walking from scalp electroencephalographic (EEG) signals. IEEE Trans. Neural. Syst. Rehabil. Eng. 20, 212-219.

Presacco, A., Goodman, R., Forrester, L., and Contreras-Vidal, J.L. (2011). Neural decoding of treadmill walking from noninvasive electroencephalographic signals. J. Neurophysiol. 106, 1875-1887.

Terao, Y., Ugawa, Y., Hanajima, R., Machii, K., Furubayashi, T., Mochizuki, H., Enomoto, H., Shiio, Y., Uesugi, H., and Iwata, N.K. (2000). Predominant activation of I1-waves from the leg motor area by transcranial magnetic stimulation. Brain Res. 859, 137-146.

Theiler, J., Eubank, S., Longtin, A., Galdrikian, B., and Farmer, J.D. (1992). Testing for nonlinearity in time series: the method of surrogate data. Phys. D *58*, 77-94.

Tibshirani, R., Walther, G., and Hastie, T. (2001). Estimating the number of clusters in a data set via the gap statistic. J. R. Statist. Soc. B *63*, 411-423.

Torres-Oviedo, G., Macpherson, J.M., and Ting, L.H. (2006). Muscle synergy organization is robust across a variety of postural perturbations. J. Neurophysiol. 96, 1530-1546.

Yokoyama, H., Hagio, K., Ogawa, T., and Nakazawa, K. (2017a). Motor module activation sequence and topography in the spinal cord during air-stepping in human: Insights into the traveling wave in spinal locomotor circuits. Physiol. Rep. 5, e13504.

Yokoyama, H., Ogawa, T., Kawashima, N., Shinya, M., and Nakazawa, K. (2016). Distinct sets of locomotor modules control the speed and modes of human locomotion. Sci. Rep. *6,* 36275.

Yokoyama, H., Ogawa, T., Shinya, M., Kawashima, N., and Nakazawa, K. (2017b). Speed dependency in α-motoneuron activity and locomotor modules in human locomotion: indirect evidence for phylogenetically conserved spinal circuits. Proc. R. Soc. B *284*, 20170290.